

Route to intense single attosecond pulses

George D Tsakiris¹, Klaus Eidmann, Jürgen Meyer-ter-Vehn
and Ferenc Krausz

Max-Planck-Institut für Quantenoptik, Hans-Kopfermann-Straße 1,
D-85748 Garching bei München, Germany
E-mail: george.tsakiris@mpq.mpg.de

New Journal of Physics **8** (2006) 19

Received 20 October 2005

Published 31 January 2006

Online at <http://www.njp.org/>

doi:10.1088/1367-2630/8/1/019

Abstract. A feasibility study is presented for the generation of single attosecond pulses using harmonics produced by planar targets irradiated at high intensities. The investigation focuses on the interaction of a few-optical cycles, carrier-envelope phase controlled, near-infrared laser pulse with an overdense plasma. The results obtained using an one-dimensional particle-in-cell code indicate that at laser intensities of 10^{20} W cm⁻² a single sub-fs pulse can be generated in the 20–70 eV spectral range with an efficiency of a few per cent and with 10^{-3} to 10^{-4} for higher photon energies.

Contents

1. Introduction	2
2. The oscillating mirror model	3
3. PIC simulations	10
4. Discussion and conclusions	18
Acknowledgments	19
References	19

¹ Author to whom any correspondence should be addressed.

1. Introduction

The basic idea in generating very short pulses is intimately connected to the superposition principle of wave mechanics, which states that spatial or temporal energy localization comes about whenever mutually coherent waves are superimposed in time and space. It is the interplay between constructive and destructive interference in a superposition of monochromatic light waves of equally spaced frequencies that manifest itself in temporal beating, the underpinning process of short pulse generation. The mathematical description of wave superposition, Fourier synthesis, indicates that the larger the number of properly phased spectral components of comparable amplitudes, the more pronounced is the confinement in time. Implementation of this concept to higher order harmonics of an optical wave offers the potential of attosecond (10^{-18} s) pulse generation [1, 2]. In this context, the nonlinear interactions of an intense optical pulse with atoms [3, 4], free electrons [5, 6] or solid surfaces [7] have been identified as most suitable sources for phase-coherent harmonic emission capable of rendering temporal confinement of light to unprecedented short timescales.

The extension of the pump-probe techniques to the extreme ultraviolet (XUV) and soft x-ray (SXR) regime based on the availability of such pulses would open the way to enormously exciting new territory and it will constitute a new approach to ultrafast science involving real-time observation of a wide range of phenomena involving fast electron dynamics (including inner-shell dynamics). Towards this goal, pulses with sufficient intensity and sub-femtosecond duration are necessary. Single sub-femtosecond XUV pulses [8, 9] as well as near-PHz repetition rate trains of such pulses [10, 11] have been demonstrated from gas targets. However, while these pulses in conjunction with intense laser pulses have allowed attosecond spectroscopy [12], they are far too weak for XUV-pump/XUV-probe spectroscopy to be successfully implemented. To this end, a new medium exhibiting stronger nonlinearities giving rise to order-of-magnitude higher harmonic efficiency and able to withstand arbitrarily high fields is in need.

Since the first observation of harmonic generation from solid targets using a tabletop laser system [13]–[15], it became apparent that the interaction of an intense laser pulse with an overdense plasma constitutes an alternative route for the efficient production of phase-locked harmonics leading to attosecond light bunching [7]. The main advantage over the process of harmonic generation in rarefied gases is that the plasma medium allows the use of higher laser intensities. Because the process of harmonic generation in an overdense plasma is of relativistic origin, the higher laser intensities induce stronger nonlinearities resulting thus in higher conversion efficiencies.

Given the rapid technological advancements in laser technology, tabletop lasers based on the Optical Parametric Chirp Pulse Amplification (OPCPA) technique [16]–[20] delivering several tens of TW power with kHz repetition rate appear to be within our reach. This new technology allows us to go even beyond this limit and envision a petawatt tabletop laser system, which would be ideally suited for the efficient generation of solid harmonics and attosecond pulses in the keV spectral range.

For a number of applications, a single attosecond pulse is desirable. While a laser pulse comprising many cycles when interacting with a nonlinear medium will in general produce a train of attosecond pulses, a few-cycle laser pulse is most appropriate for the generation of a single attosecond pulse. The reproducibility of the generation process of a single attosecond pulse has been greatly improved with the attainment of carrier-envelope phase stabilization, which allows precise timing of the field oscillations within the pulse envelope [21, 22]. Waveform control is

actually a prerequisite for the generation of single attosecond pulses because, due to the high nonlinearity of the process, by suitably adjusting the carrier-envelope phase only one cycle under the envelope contributes to the emission of harmonic radiation within a selected spectral range. This has been demonstrated for the case of the atomic harmonics from gas targets [21], but not yet for solid harmonics from overdense plasma. The advantage in using solid harmonics instead is by the orders of magnitude higher expected intensity of the attosecond pulses. This will not only greatly ease their characterization, but also significantly expand the scope of their applications.

Motivated by the prospects offered by the rapidly evolving laser technology, we have used the one-dimensional particle-in-cell (PIC) code laser particle-in-cell (LPIC) [23] and looked into the possibility of producing single attosecond pulses using the harmonic emission emanating from the interaction of intense few-cycle laser pulses with overdense plasmas. In our simulations, a two-cycle (Gaussian-FWHM) p-polarized laser pulse is incident at 45° onto a planar target consisting of 80 times overdense plasma for the $\lambda_L = 0.8 \mu\text{m}$ laser wavelength. The most important parameter pertaining to this interaction is the normalized field amplitude or normalized vector potential of the incident laser pulse defined as $a_L = eE_L/(\omega_L mc) = eA_L/(mc)$. In terms of the laser intensity I_L and wavelength λ_L is given as $a_L^2 = I_L \lambda_L^2 / (1.37 \times 10^{18} \text{ W } \mu\text{m}^2 \text{ cm}^2)$ and it was varied between $a_L = 3$ –100 corresponding to a laser intensity range of $I_L = 2 \times 10^{19}$ to $2 \times 10^{22} \text{ W cm}^{-2}$. This intensity range covers the present day capabilities in laser technology as well as those envisaged for the near future [24]. Another approach for generating single attosecond pulses using intense, tightly focused laser pulses has been reported by Naumova *et al* [25]. This method relies on two-dimensional effects arising from a small focal spot of the order of the laser wavelength. The method described in this report assumes a larger focal spot several wavelengths in diameter so that the initial plasma expansion is planar. This justifies in turn the use of the one-dimensional LPIC code employed in the simulations reported in this paper.

As in the case of gas harmonics, the power spectrum of the specularly reflected light from an overdense plasma exhibits a maximum frequency and a characteristic roll-off. In contrast however, the maximum frequency increases with the laser intensity without any limitation (no saturation intensity) and the roll-off shows a power-law dependence without any plateau region. The common procedure to generate shorter pulses from these type of power spectra is to exclude the low frequency harmonics that dominate and consequently restrict the available bandwidth by using a high-pass filter. It becomes apparent that the characteristic roll-off of the spectrum would then play an important role in generating for a given intensity the shortest possible pulse with the maximum efficiency. Furthermore, a similar sensitivity like in the case of atomic harmonics to the absolute envelope-carrier is observed. Pulses with two maxima of the laser field tend to generate two attosecond pulses while pulses with a single maximum generate a single one.

2. The oscillating mirror model

A very useful model that provides insight into the mechanism of high harmonic generation at high intensities in solid targets is the so-called *oscillating mirror* model. It was first proposed by Bulanov *et al* [26] and later formulated and developed in detail by Lichters *et al* [23]. Since then, it has been used in a series of reports dealing with the harmonic generation process from the interaction of intense laser pulses with solid surfaces. More recently, very important additional insight in the theoretical aspects of the model has been obtained by Gordienko *et al* [27], who

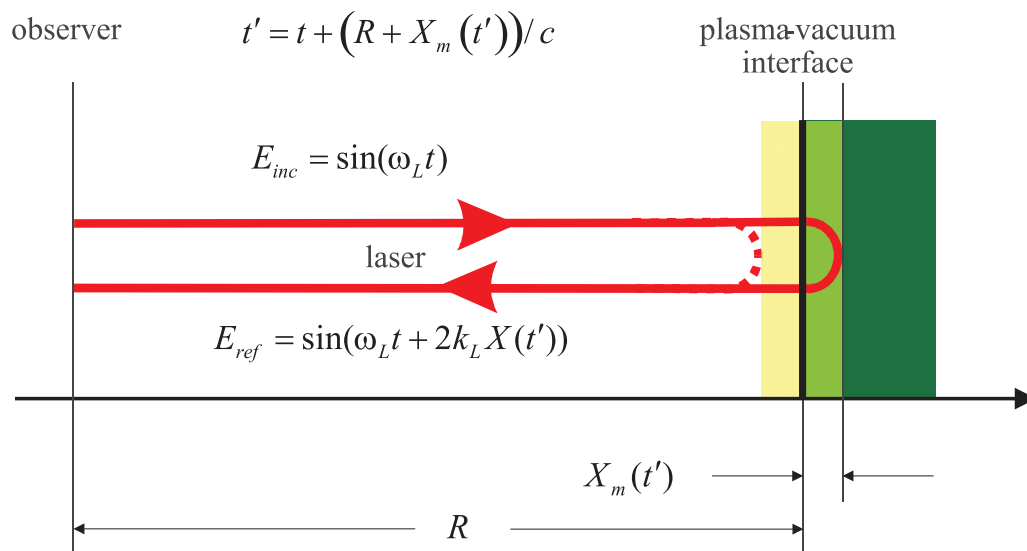


Figure 1. Scheme showing the basic idea of the oscillating mirror model. An E-M wave is incident on an electron surface oscillating around an immovable ion background. The phase of the reflected E-M wave as seen by the observer depends on the position of the electron surface at the moment of the reflection. This retardation effect gives rise to a distorted waveform rich in harmonics of the fundamental frequency.

could deduce in rather general terms a universal scaling for the roll-off of the harmonic spectrum in power-law form $I(\omega) \propto \omega^{-q}$ with $q \approx 5/2$. They also showed that the harmonic spectrum extends up to a maximum cut-off frequency $\omega_{co} \approx 4\gamma_{max}^2 \omega_L$, where ω_L is the incident laser frequency and γ_{max} denotes the relativistic γ -factor corresponding to the maximum velocity at which the mirror moves towards the incoming light. The factor $4\gamma_{max}^2$ relates to the basic underlying mechanism which is Compton backscattering of light on a relativistic mirror. For the laser-driven mirror, consisting of oscillating overdense electron ensembles at the irradiated surface of a solid, the emission of high-frequency photons as seen by the observer occurs only during small fractions of the fundamental laser period T_L of the order of $\Delta t \approx T_L/4\gamma_{max}^2$. In the time domain, this leads to a train of high-frequency photon bursts which transforms into the high harmonics spectrum in frequency space. For few-cycle driving pulses, even single electromagnetic spikes of attosecond duration can be created. Gordienko *et al* found that these theoretical results are in excellent agreement with 1D-PIC simulations.

The intention of the present paper is to discuss these results in the context of near-term experiments. In this section, we rederive the model in elementary terms and illustrate the salient features such as power-law spectrum, cut-off and attosecond spikes by using a simple analytical expression for the mirror motion. By exploiting the simple analytical expressions for the power law and cut-off harmonic, we proceed to deduce estimates for the efficiency and duration of the short pulses that can be generated by this process.

The basic idea of the model is depicted in figure 1. It assumes that the electrons at the plasma vacuum interface execute forced oscillations near the edge of an immobile step-like ion background driven by the ponderomotive force of the incident laser pulse. Its origin is the $\vec{v} \times \vec{B}$ term of the Lorentz force, and its oscillatory term varies as $F_p(t) \sim I_L \lambda_L^2 \sin(2\omega_L t)$. Charge

separation and corresponding electrostatic fields give rise to the restoring force. As it has been pointed out by Lichters *et al* [23], one of the main reasons for the rich harmonic content in the reflected pulse is the retardation effect between a point of reference (observer) and the electron interface on which the incident wave is reflected. Denoting by $X_m(t')$ the mirror motion, the field crossing at time t the observer position will arrive at the mirror at a later time given by $t' = t + (R + X_m(t'))/c$ where R is the distance between observer and plasma-vacuum interface (see figure 1). This gives the relation between the retarded time t' and the observer's time t as

$$t' = t + X_m(t')/c. \quad (1)$$

Here we have omitted the constant term R/c since it represents a time-independent phase shift of no consequence in calculating the field of the reflected wave. After a complete round trip the total time upon arrival back at the observer's reference position is thus $t + 2(t' - t) = t + 2(R + X_m(t'))/c$. Consequently, the incident field $E_{\text{inc}}(t) = \sin(\omega_L t)$ gives rise to a reflected field $E_{\text{ref}}(t) = \sin(\omega_L t + 2k_L X(t'))$, where we have omitted again the time-independent phase shift $2k_L R$. This expression has been derived from simple kinematic considerations and shows explicitly an important nonlinearity involved in the process. This is clearly a source of harmonic generation. More realistic PIC simulations of the process incorporate self-consistently the additional nonlinearities that contribute even further to harmonic production due to relativistic effects at high intensities.

The mirror position $X_m(t')$ bouncing the wave back is generally an unknown function. However, based on the fact that the driving ponderomotive force is harmonic with frequency twice that of the incident laser, to a first approximation a form $X_m(t') = A_m \sin(2\omega_L t' + \phi_m)$ can be assumed. Here, A_m is the amplitude of the oscillation and ϕ_m is the relative phase between the incident wave and the mirror position. After thus specifying the functional form for the mirror motion, the implicit equation for the retarded time can be numerically evaluated and the temporal evolution of the reflected wave obtained. If the retardation effect can be neglected, we have $t \approx t'$ and the reflected field is simply phase modulated. In this case the spectrum can be expressed in terms of Bessel functions. At high intensities however the mirror motion is highly relativistic (velocities approaching c) and the retardation effect cannot be disregarded. As discussed in the following, the corresponding spectrum in this case is more complicated. The amplitude A_m of the oscillation is estimated as follows: the maximum velocity of the mirror is $v_{\text{max}}/c = \beta_{\text{max}} = 2A_m\omega_L/c$. In terms of the relativistic factor $\gamma_{\text{max}} = 1/\sqrt{1 - \beta_{\text{max}}^2}$, the oscillation amplitude can be expressed as $A_m = \frac{\lambda_L}{4\pi} \sqrt{\gamma_{\text{max}}^2 - 1}/\gamma_{\text{max}}$. For the case of a relativistic fluid plasma the relativistic factor γ_{max} is connected to the normalized vector potential through the relation $\gamma_{\text{max}} = \sqrt{1 + a_L^2}$ [28]. In terms of the normalized vector potential the expression for the mirror motion takes now the form

$$X_m(t') = \frac{\lambda_L}{4\pi} \frac{a_L}{\sqrt{1 + a_L^2}} \sin(2\omega_L t' + \phi_m). \quad (2)$$

For a given a_L and ϕ_m the reflected field is thus completely specified and its Fourier transform gives the power spectrum predicted by the oscillating mirror model. An example is given in figure 2 for $a_L = 10$ and $\phi_m = 0$. The time it takes the mirror to sweep through a half-period of the reflected field is dilated by a factor $4\gamma_{\text{max}}^2$ when the mirror and the wave co-propagate whilst it is contracted by the same factor when they counter-propagate. For high values of a_L the velocity

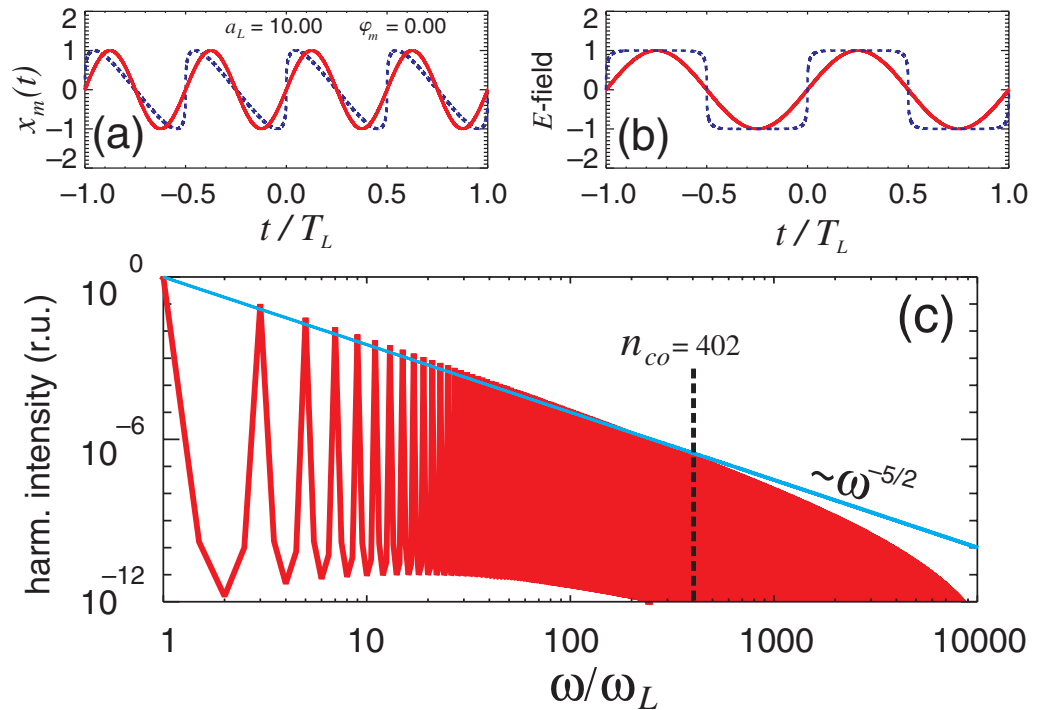


Figure 2. Predictions of the oscillating mirror model for $a_L = 10$. (a) Motion of the mirror in its own frame (—) and as seen by the incident wave (---). (b) The incident (—) and the reflected (---) E-M field as seen by the observer. (c) The power spectrum is obtained by Fourier transforming the reflected field. The roll-off follows closely the predicted power law $1/\omega^q$ with $q \approx 5/2$. The value for the cut-off harmonic n_{co} is calculated using equation (3).

associated with the motion is close to c and for the particular choice of the mirror phase $\phi_m = 0$ this effect gives rise to the nearly square-like waveform of the reflected wave shown in figure 2(b). It is a consequence of the fact that the wave for a half laser period is reflected at constant phase by the moving mirror.

The power spectrum of the harmonic emission is also shown in figure 2. It contains only odd harmonics and rolls off according to the power law $1/\omega^q$ up to a cut-off harmonic n_{co} where a near exponential intensity drop for higher harmonics is observed. It is interesting to note that the universal power law for $q = 5/2$ reported in [27] is in good agreement with the results obtained for the specific choice $X_m(t') = A_m \sin(2\omega_L t' + \phi_m)$ for the mirror motion with $\phi_m = 0$. It is found that a choice for the mirror oscillatory motion with the fundamental frequency ω_L , i.e., $X_m(t') = A_m \sin(\omega_L t' + \phi_m)$ produces a spectrum containing all the harmonics but the same power-law roll-off. Change of the phase ϕ_m to another value $\phi_m \neq 0$ has some influence on the roll-off of the spectrum: the exponent in the power law varies continuously from $q \approx 5/2$ for $\phi_m = 0$ to $q \approx 3$ for $\phi_m = \pi$. As is discussed in section 3, PIC simulations that self-consistently calculate the vacuum-plasma interface motion produce a power spectrum exhibiting a power-law roll-off with $q \approx 5/2$. It appears therefore that the wave and the mirror are in phase ($\phi_m = 0$) and the reflection of the incident wave occurs when the field is at its maximum.

The cut-off frequency ω_{co} corresponds to the maximum angular frequency contained in the reflected pulse and is obtained from $\omega_{\text{co}} = \max(d\Phi_{\text{refl}}/dt)$, where $\Phi_{\text{refl}} = \omega_L t + 2k_L X(t')$ is its phase. Taking into account that $t = t' - X_m(t')/c$, we find $dt/dt' = 1 - \beta(t')$ and $\omega_{\text{co}} = \omega_L(1 + \beta_{\text{max}})/(1 - \beta_{\text{max}}) \approx 4\gamma_{\text{max}}^2 \omega_L$ for relativistic $\gamma_{\text{max}} \gg 1$, as derived before by Gordienko *et al* [27]. The cut-off harmonic n_{co} depends thus on the laser intensity and as a function of the normalized vector potential is given by:

$$n_{\text{co}} = \frac{\sqrt{1 + a_L^2} + a_L}{\sqrt{1 + a_L^2} - a_L} \xrightarrow{a_L \gg 1} 4a_L^2 \approx 4\gamma_{\text{max}}^2. \quad (3)$$

This expression applied to the specific case of figure 2c gives the value of $n_{\text{co}} \approx 402$. As seen, it accurately predicts the change in the slope exhibited by the corresponding power spectrum. It is interesting to note that for high laser intensities the cut-off harmonic scales quadratically with the normalized vector potential $a_L^2 \sim I_L \lambda_L^2$ as in the case of harmonics from an atomic medium.

Generally, the spectrum is discrete and contains multiples of the fundamental (laser) frequency. For short laser pulses comprising merely a few laser cycles, the harmonics are broad and they tend to overlap, giving rise to a quasi-continuum spectrum especially towards the high-frequency end. In order to deduce some scaling laws of interest, we assume a continuous power spectrum for the reflected light of the form $I_{\text{ref}}(\omega) = dP_{\text{ref}}(\omega)/d\omega \propto 1/\omega^q$ with $P_{\text{ref}}(\omega)$ the reflected power. As is discussed in more detail in section 3, the generation of attosecond pulses results from slicing out a part of the harmonic spectrum using a band-pass filter between two frequencies ω_{min} and ω_{max} . The simple analytical form of the reflected spectrum allows us to derive an estimate for the efficiency η_{XUV} of the attosecond pulse. This can be calculated from

$$\eta_{\text{XUV}} = \frac{1}{P_{\text{inc}}} \int_{\omega_{\text{min}}}^{\omega_{\text{max}}} \frac{dP_{\text{ref}}(\omega)}{d\omega} d\omega, \quad (4)$$

where the incident power is approximated by the total reflected power, i.e., $P_{\text{inc}} \approx P_{\text{ref}} = \int_0^\infty \frac{dP_{\text{ref}}(\omega)}{d\omega} d\omega$. The PIC simulations show that indeed a very small amount of the incident light is absorbed by the plasma and more than 96% is reflected in the fundamental and its harmonics (see section 3). Given that the spectrum does not extend to infinity but up to the cut-off harmonic n_{co} , and considering now a high-pass filter allowing harmonics higher than n_F to be transmitted, the following expression for the XUV efficiency can be readily derived from equation (4) by setting $\omega_{\text{min}} = n_F \omega_L$ and $\omega_{\text{max}} = n_{\text{co}} \omega_L$:

$$\eta_{\text{XUV}} = \frac{n_{\text{co}}^{q-1} - n_F^{q-1}}{n_F^{q-1} (n_{\text{co}}^{q-1} - 1)} \xrightarrow{n_{\text{co}} \gg n_F} \frac{1}{n_F^{q-1}}. \quad (5)$$

For high laser intensities so that $n_{\text{co}} \gg n_F$ and for $q = 5/2$, the mirror model thus predicts the astonishingly simple result

$$\eta_{\text{XUV}} \sim n_F^{-3/2}. \quad (6)$$

The importance of the power-law roll-off becomes apparent in figure 3(a) where the estimated efficiency as given by equation (5) for $a_L = 10$ and for three different values of the

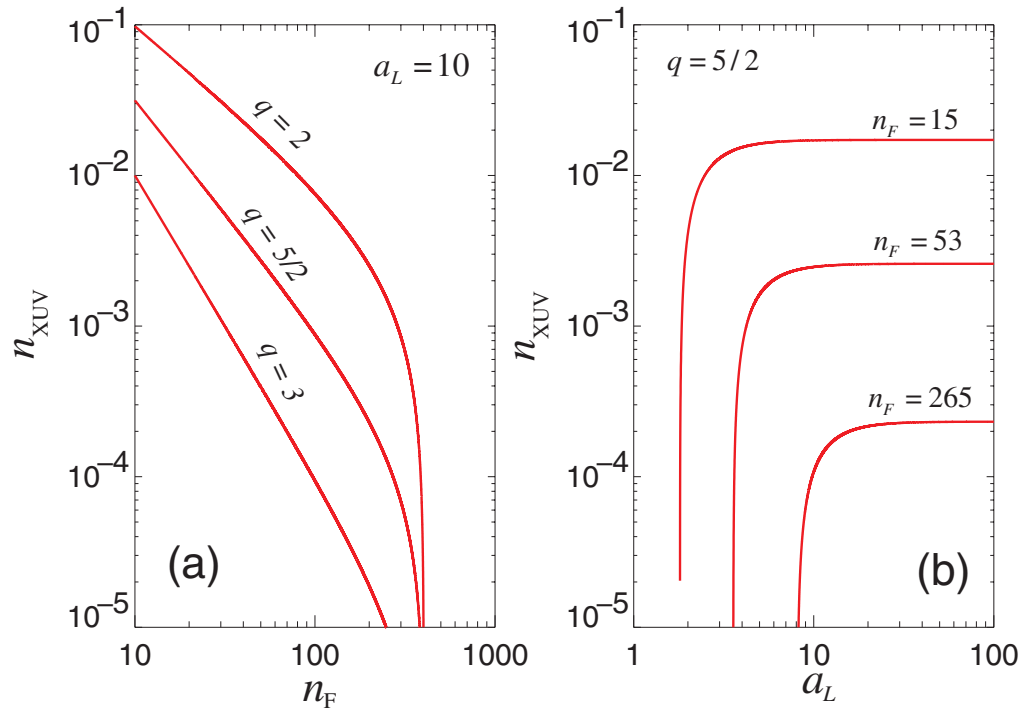


Figure 3. The efficiency η_{XUV} for the conversion of the laser light into XUV attosecond pulses (a) as a function of the filter cut-off harmonic n_F for $a_L = 10$ and three values of the exponent q and (b) as a function of the normalized filed amplitude a_L for $q = 5/2$ and the indicated filter cut-off harmonic n_F . In both cases the XUV efficiency is calculated using equation (5) in combination with equation (3).

exponent q is plotted. It is seen that the efficiency strongly depends on the exponent of the roll-off of the harmonic spectrum. For the value $q = 5/2$ predicted by the mirror model the conversion efficiency into an XUV pulse reaches even the few per cent level. In figure 3(b) the dependence of η_{XUV} on a_L is given for three values of the filter cut-off harmonic n_F corresponding to the lowest harmonic transmitted through the thin foil filters discussed in section 3. The main feature that the PIC simulations confirm is the saturation of the efficiency for high intensities (large values of a_L) at the value $\eta_{\text{XUV}} \approx 1/n_F^{q-1}$. This can be attributed to the saturation of the efficiency starting with the low lying harmonics. Simultaneously however, higher harmonics are generated more efficiently giving rise to an increase in the efficiency of harder XUV pulses (see also discussion of figure 11 in section 3). Although this represents only a rough estimate it nevertheless underlines the significant difference in the conversion efficiency to higher harmonics in a plasma medium compared to a gas medium.

One aspect of interest in relation to the topic of this report is the influence of the power spectrum roll-off to the duration of the XUV pulses. The question that naturally arises is: what is the shortest XUV pulse that can be achieved by a power-spectrum with a power-law roll-off for a given laser intensity (specific a_L) and what part of the spectrum should be used to this end? The simple analytical expression for the power spectrum can be used to provide an answer. We have calculated the intensity of the filtered pulse I_{XUV} by taking the inverse Fourier transform of the

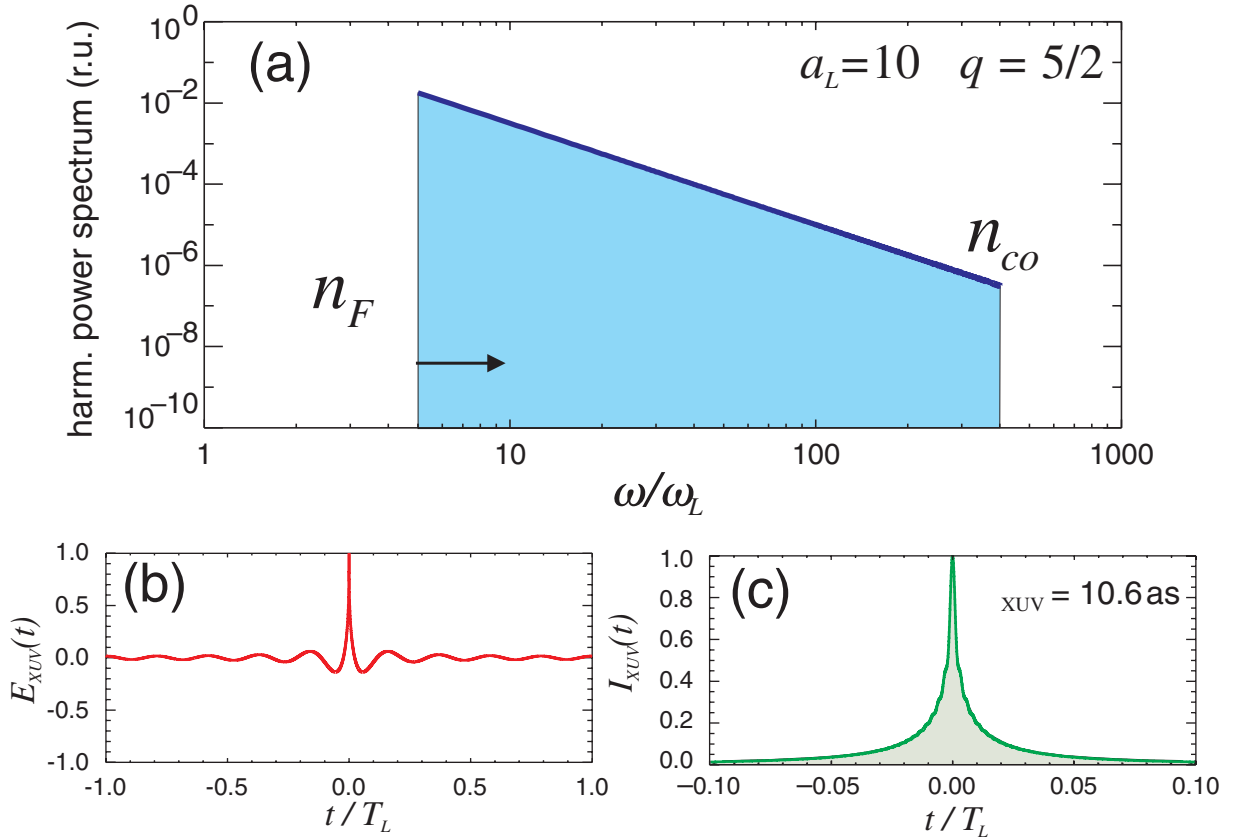


Figure 4. The continuous power spectrum with power-law roll-off $1/\omega^{5/2}$ between the harmonics $n_F = 5$ and $n_{co} = 402$ shown in (a) gives rise to a XUV pulse in the time domain with a normalized E-field shown in (b) and intensity shown in (c).

harmonic field $E_{XUV}(t) = \mathcal{F}^{-1}\{\sqrt{I(\omega)}\}$. In doing so, we have tacitly assumed Fourier transform limited pulse, an assumption that the PIC simulations corroborate (see section 3). Figure 4, shows an example of this procedure for $a_L = 10$, $q = 5/2$ and $n_F = 5$. The model spectrum is terminated at the cut-off harmonic given by equation (3). In this case, the Fourier synthesis of the coherent spectrum assumed by the model gives rise to an XUV pulse of duration $\tau_{XUV} \approx 10.6$ as.

The dominant frequencies in the pulse are those close to the cut-off frequency of the filter. For a fundamental laser beam consisting of photons with 1.51 eV energy, a high-pass filter with $n_F = 5$ means that the attosecond pulse will comprise mainly 8 eV photons, i.e., its carrier frequency will be in the 40 nm spectral range. For some applications a different spectral range is desirable containing more energetic photons. In this case another high-pass filter with a higher transmission frequency should be used. This inevitably will influence the pulse duration in a matter that is closely connected to the characteristics of the spectrum and more specifically to its roll-off. To illustrate this, we have varied the frequency of the high-pass filter from $n_F = 5$ to 1000 and calculated the corresponding duration of the thus generated XUV pulse for three different laser intensities and three values of q in the relation $I(\omega) \sim 1/\omega^q$. The results are depicted in figure 5. It is seen that for increasing values of n_F the duration at the beginning decreases. This

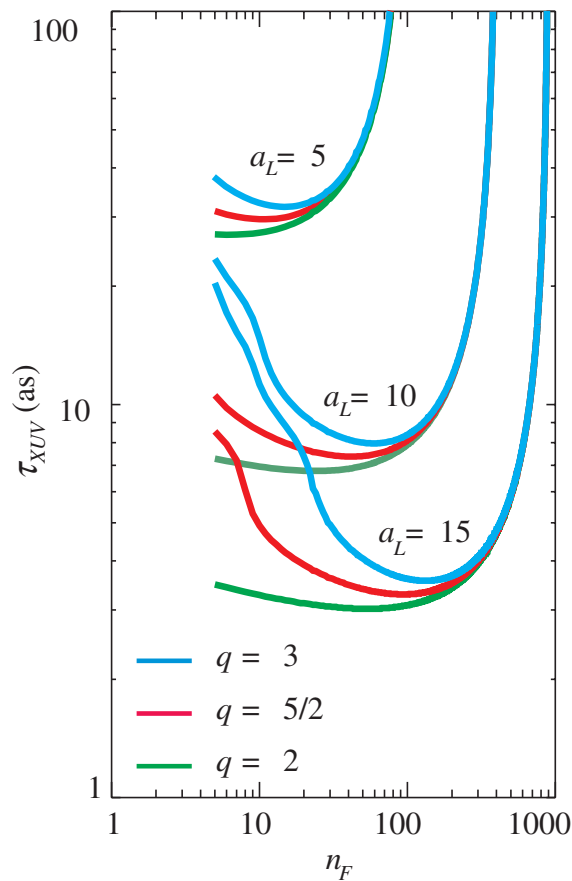


Figure 5. The XUV pulse duration as a function of the filter cut-off harmonic for the indicated power-law exponent q and normalized vector potentials a_L .

is at first counterintuitive because one would expect longer pulse duration for less bandwidth. The half-intensity bandwidth for the power-law spectrum $I(\omega) \sim 1/\omega^q$ is easily seen to vary as $\Delta n_{1/2} = (2^{1/q} - 1)n_F$, thus it increases for larger values of the filter cut-off harmonic n_F . As long as $n_F \ll n_{co}$ due to the steep drop of the power spectrum, the effect of the cut-off harmonic n_{co} to the pulse duration is negligible. It is only when $n_{co} - n_F \lesssim \Delta n_{1/2}$ that the reduction in the bandwidth results again in broader pulses. It appears that for a given value of q and a_L there is an optimum filter frequency that would give the shortest possible pulse. For example for $q = 5/2$ and $a_L = 10$ a high-pass filter with $n_F \simeq 50$ will produce an XUV pulse comprising photons in the 300 eV range and duration $\tau_{XUV} \simeq 8$ as while for $a_L = 15$ the duration will be in the $\tau_{XUV} \simeq 3$ as range.

3. PIC simulations

PIC codes are well-established tools for kinetic simulations in plasma physics. Numerical kinetic treatment has provided new insights in a number of topics related to the interaction of high intensity pulses with plasmas. More specifically, they have helped to understand some intricacies associated with the generation mechanism of high harmonics at overdense plasma surfaces

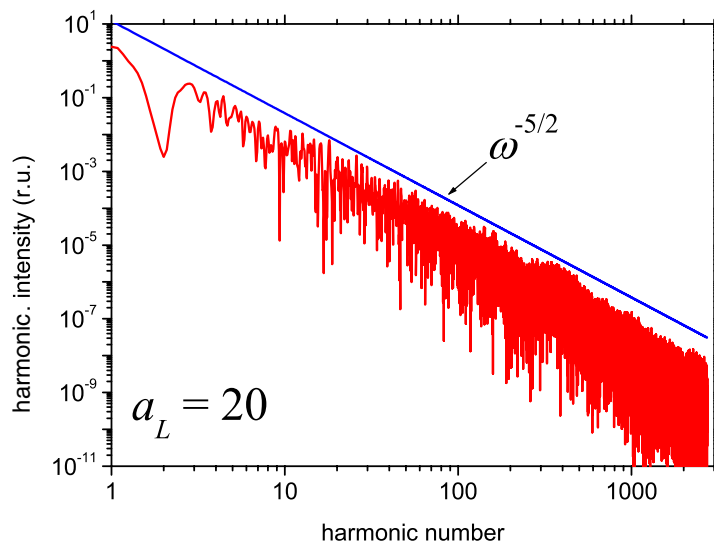


Figure 6. Harmonic power spectrum as calculated with the LPIC code for initial conditions close to those assumed in the oscillating mirror model. The power-law roll-off $1/\omega^{5/2}$ is clearly reproduced.

[15], [29]–[31]. Thus, their appropriateness in predicting new phenomena in previously unexplored laser intensities is well justified.

In this section, we present results obtained by the 1D code LPIC [23] in a parameter range, which is expected to provide intense isolated attosecond pulses in the XUV or even SXR spectral range. As a first step, using LPIC, we have verified the predictions of the mirror model regarding the roll-off of the power spectrum. The results of this simulation are depicted in figure 6 and the initial conditions are such as to match the assumptions inherent in the model. They include a step-like initial electron and ion density profile, immobile ions, and normal angle of incidence. The rest of the initial conditions are a two-cycle (Gaussian) laser pulse with normalized vector potential $a_L = 20$ incident on a planar target. It is seen that under these conditions the power spectrum obtained from the LPIC code matches well the $1/\omega^{5/2}$ power law predicted by the mirror model and reported by Gordienko *et al* [27].

To investigate the conditions under which harmonic combs generated by solid targets yield attosecond pulses, in what spectral range and with which efficiency, we have performed a series of simulations. We have used initial conditions as close as possible to an envisioned experimental configuration, which is schematically shown in figure 7. It resembles the most common experimental setup utilized in a number of previous experiments [13]–[15]. The limitations and the restrictions in approaching the actual experimental configuration are mainly due to computing capacity and they are discussed in the last section. In the rather simple setup depicted in figure 7, a phase stabilized, two-cycle ($\lambda_L = 0.8 \mu\text{m}$, $\tau_L \sim 5$ fs) laser pulse, with a Gaussian envelop and p-polarization is focused at 45° on a planar target consisting of 80 times overdense plasma for the $0.8 \mu\text{m}$ laser wavelength. These initial conditions were kept constant throughout the simulations.

The intense laser pulse interacts with a plasma characterized by a sharp density gradient and is reflected in the specular direction. The normalized vector potential was varied between $a_L = 3$ –100 corresponding to a laser intensity range of 2×10^{19} to 2×10^{22} W cm $^{-2}$ for

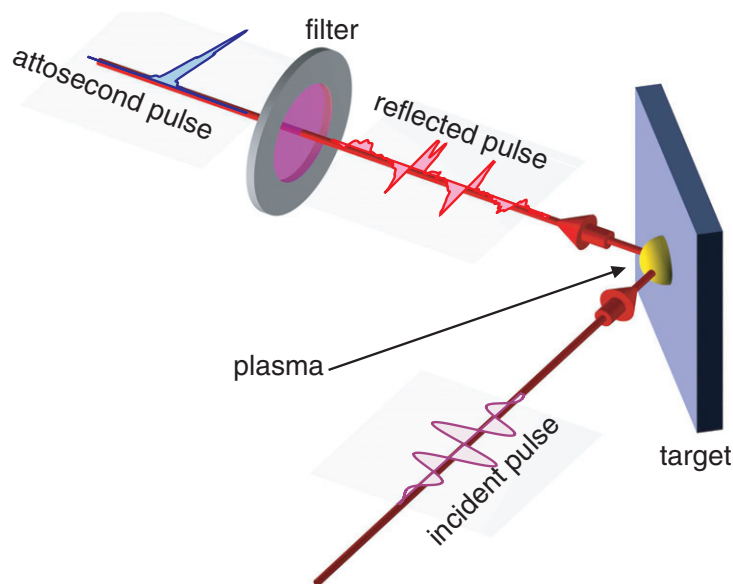


Figure 7. Scheme showing the proposed experimental configuration for the generation of attosecond pulses using harmonics from overdense plasmas.

$\lambda_L = 0.8 \mu\text{m}$. Although most of the simulations were performed with a step-like electron and ion density profile, we have also used an exponential density profile of a given scale-length L in order to investigate the effect of preformed plasma. As it was pointed out in section 2, passing the reflected pulse through an appropriately thin metal foil results in filtering the low frequencies and thus generating attosecond pulses. As it is discussed later on, it is mainly the combination of filter material and laser intensity that determines the spectral range and the duration of the attosecond pulses. The effect of the carrier-envelope phase on the filtered pulses has been studied by varying the absolute phase ϕ between 0 (sine pulse) and $\pi/2$ (cosine pulse).

In figure 8 the spatiotemporal behaviour of the electron density profile is shown during the interaction of a two-cycle cosine pulse of intensity $2 \times 10^{19} \text{ W cm}^{-2}$ ($a_L = 3$) with a preformed plasma possessing a scale-length $L = \lambda/4$. Upon arrival of the laser pulse the electrons start executing strong and rather complicated excursions around the critical density $\omega_L = \omega_p$ surface. The motion is certainly highly nonlinear resulting in a distorted reflected pulse rich in harmonic content. This is depicted in the plots to the left of figure 8 where the incident and reflected pulse in time-domain are shown. The tendency towards generating shorter pulses becomes evident by the *sharpening* of the half-cycle peaks in the reflected pulse. Although some of these peaks exhibit durations in the range of a few hundred attoseconds, they are not the attosecond pulses sought for since they do not possess a carrier frequency.

As in the case of atomic harmonics [32], use of a high-pass filter that absorbs the fundamental and the lower harmonics gives rise to pulses shorter than the laser half-period. In section 2 the process was studied in terms of the mirror model. Here, we apply the same method to the simulations results using realistic filters consisting of $0.2 \mu\text{m}$ thick Mg, Al, Zr or Cu metal foils. The choice is such as to select different frequency ranges starting from low to high energy photons. The result of filtering of the reflected radiation produced by a cosine $\phi = \pi/2$ laser pulse with intensity $7 \times 10^{20} \text{ W cm}^{-2}$ ($a_L = 20$) on a step-like density profile is shown in a comprehensive way in figure 9. The first column contains the incident and the reflected pulse in the time domain

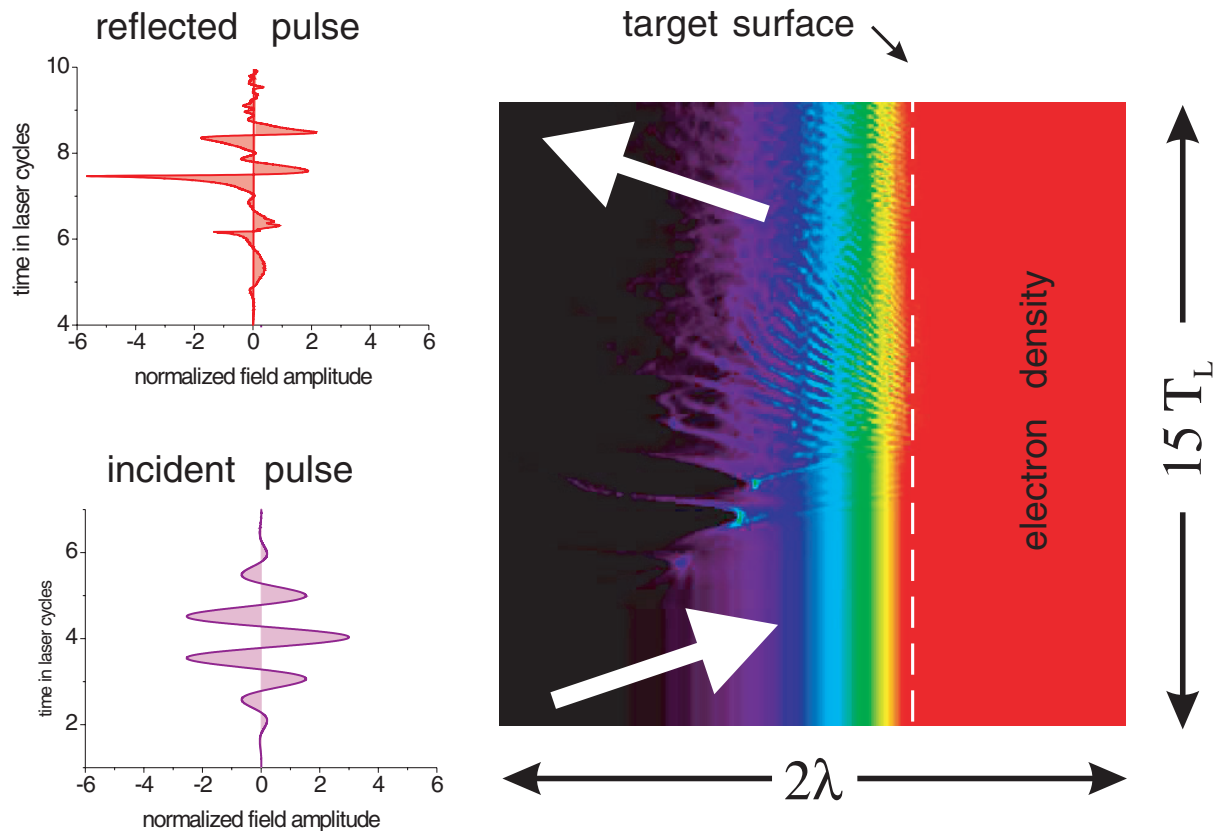


Figure 8. Spatiotemporal variation of the electron density during the interaction of a two-cycle pulse of $a_L = 3$ with a preformed plasma having a scale-length $L = \lambda/4$. The colours represent the density variation in linear scale. The temporal variation of the incident and reflected pulse is shown on the left.

as well as the temporal evolution of the E-field and the corresponding instantaneous intensity of the filtered pulse for the four filters chosen. The numerical procedure used to obtain the filtered pulse data is by convoluting the reflected pulse with the response function of the filter in the time domain. The second column gives the same information in the frequency domain. The reflected pulse spectrum exhibits a rich harmonic content and a linear spectral phase variation with frequency. This justifies the assumption of Fourier transform limited pulse made in section 2. By integrating the spectrum of the incident, reflected and filtered pulse the efficiency η_{ref} of the total reflected power and the efficiency η_{XUV} of the conversion into the filtered pulse with respect to the incident power is estimated. The third column is a blow-up of the instantaneous intensity of the filtered pulse for each of the filter material considered. The duration τ_{XUV} of the resulting attosecond pulse is estimated by fitting a gaussian pulse to the instantaneous intensity of the filtered pulse. It is noted here that this duration estimate does not take into account possible corrections due to the dispersive properties of the filters.

The first observation is that even at 45° angle of incidence the power spectrum (second column in figure 9) still rolls off according to the power law $1/\omega^q$ with q very close to the $5/2$ value. Due to the nonzero angle of incidence, the component of the electric field of the p-polarized wave perpendicular to the planar interface is the dominant driving force of the oscillations thus

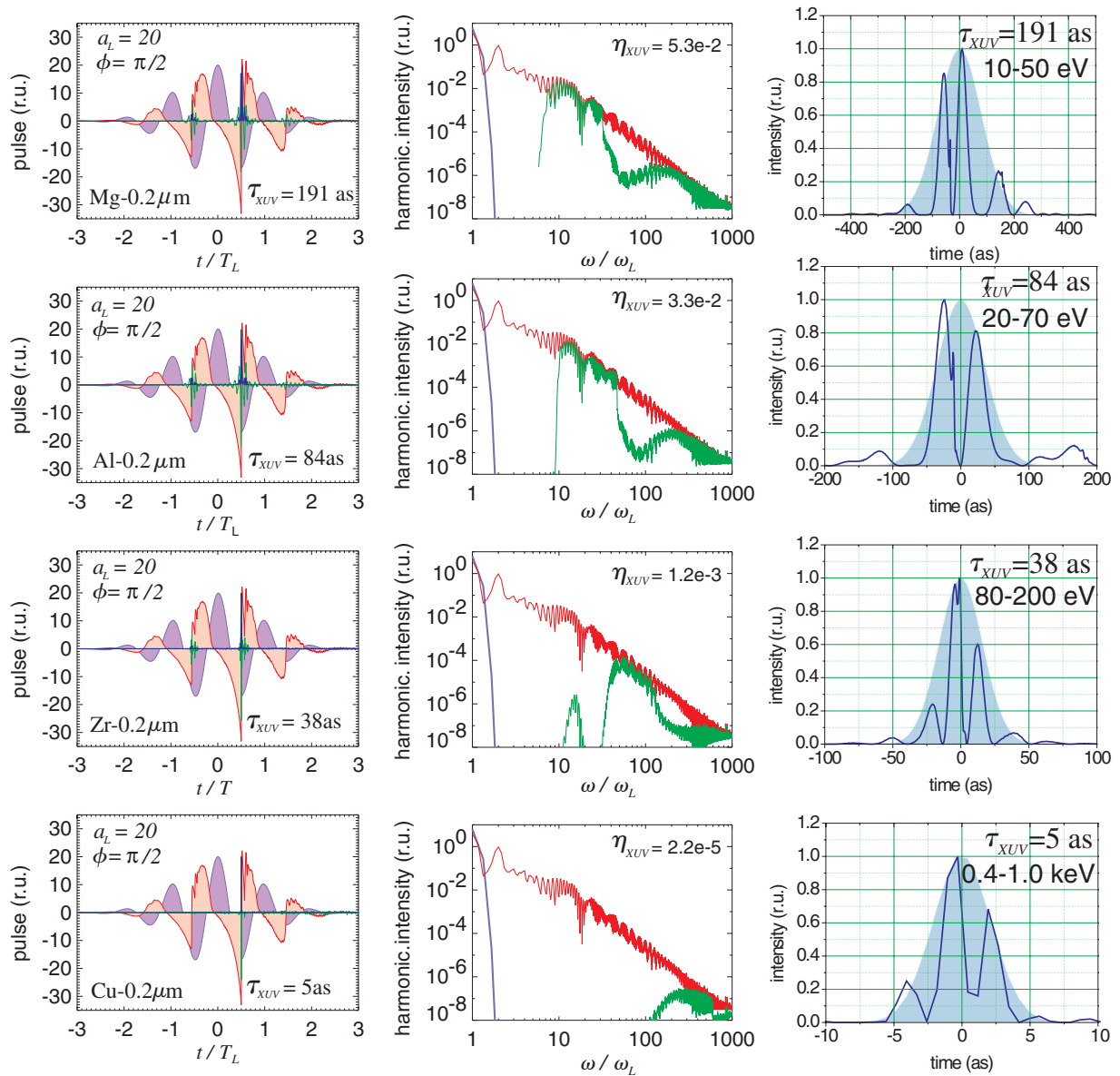


Figure 9. LPIC code simulation of the interaction of a two-cycle cosine ($\phi = \pi/2$) pulse of $a_L = 20$ incident at 45° on a step-like density profile and the resulting attosecond pulses for various filters. Left column: the incident (purple shaded area), reflected (red shaded area) and filtered pulse (green line: electric field, blue line: instantaneous intensity). Middle column: in frequency domain the incident (purple line), reflected (red line) and filtered pulse (green line). The reflected pulse has been convoluted with the transmission function of $0.2 \mu\text{m}$ thick Mg, Al, Zr and Cu to obtain the attosecond pulses resulting after filtering. The conversion efficiency η_{XUV} for the different filters is given in the corresponding figure of the middle column. The total conversion efficiency (no filtering) for this case is $\eta_{\text{ref}} = 0.96$. Right column: a blow-up of the instantaneous intensity of the attosecond pulses produced through the corresponding filter. The shaded area is a Gaussian pulse fit to obtain the duration for each case.

all harmonics (odd and even) are produced. Furthermore, it is seen that indeed by filtering the reflected pulse short pulses with durations of few hundred down to few attoseconds are produced. The appearance of these pulses coincides with the fastest temporal change in the E-field of the reflected pulse. This supports the basic idea of generating single attosecond pulses by controlling the absolute carrier-envelope phase ϕ of the pulse so that only one occurrence of such attosecond burst occurs. The total conversion efficiency η_{ref} is $\sim 96\%$ indicating that at these intensities most of the pulse energy is reflected back and very little is absorbed by the plasma of the target. The efficiency of conversion into the XUV pulse after filtering on the other hand depends on the filter material and therefore on the energy of the reflected photons. As expected, for low energy photons obtained through filtering with Mg this efficiency is the highest approaching values of a few per cent whereas for Cu filter material this efficiency is of the order of 10^{-5} .

The detailed structure of the XUV pulse shown in the third column of figure 9 reveals that as expected the carrier frequency corresponds approximately to the dominant photon energy transmitted by each filter. Similarly, the photon energies present in the XUV pulse are determined by the transmission characteristics of each filter in combination with the reflected spectrum for a given a_L . For the case in figure 9, for Mg filter the XUV pulse comprises photon energies in the range of 10–60 eV with a bandwidth giving rise to 192 as pulses while the Al filter 20–70 eV and 84 as, the Zr 80–200 eV and 38 as and the Cu 400–1000 eV and 5 as correspondingly. It should be noted here that the duration τ_{XUV} of the attosecond burst depends predominantly on the filter transmission characteristics but also on the intensity of the incident pulse. For the same filter, the reflected power spectrum changes with increasing a_L with the tendency higher harmonics to be more efficiently generated and therefore an effective broader bandwidth to become available thus producing shorter pulses.

Assuming that the possibility to vary the carrier-envelope absolute phase ϕ exists for the intensities we have considered in this paper, its influence in controlling the number of the attosecond pulses produced for a given combination of laser intensity and filter material is instrumental. For the case of figure 9 and for the Al and Zr filters, we have calculated the XUV pulses produced in the case of a sine pulse $\phi = 0$ and in the case of a cosine pulse $\phi = \pi/2$. The results are presented in figure 10. Two XUV pulses of nearly equal intensity are produced when two maxima of equal amplitude are present in the incident pulse (sine pulse $\phi = 0$), whereas for an incident pulse with a single maximum (cosine pulse $\phi = \pi/2$) the first XUV pulse is almost entirely suppressed. This behaviour is akin to the case of atomic harmonics [21] and it is due to the high nonlinearity of the process of generation. It is found that the higher the photon energy in the XUV pulse, the more effective the control through ϕ of the degree of suppression of one of the peaks.

Perhaps the most interesting result of this investigation is the efficiency with which these attosecond XUV pulses are produced. In a series of simulations in which the intensity of the incident pulse was varied but all other input parameter were kept constant we have calculated the efficiency η_{XUV} as a function of the normalized vector potential a_L for three of the filter materials considered (Al, Zr and Cu). The results averaged over the two values $\phi = 0$ and $\phi = \pi/2$ of the carrier-envelope absolute phase are given in figure 11. In deviation to the other simulations presented earlier in this paper, the electron density profile used in these simulations is exponential with a scale-length $l = \lambda/4$. The reason is that the XUV efficiency greatly improves over the step-like density profile when a preplasma with a relative small scale-length $l \lesssim \lambda$ is present. Similar effect has been reported earlier for many-cycle pulses [15].

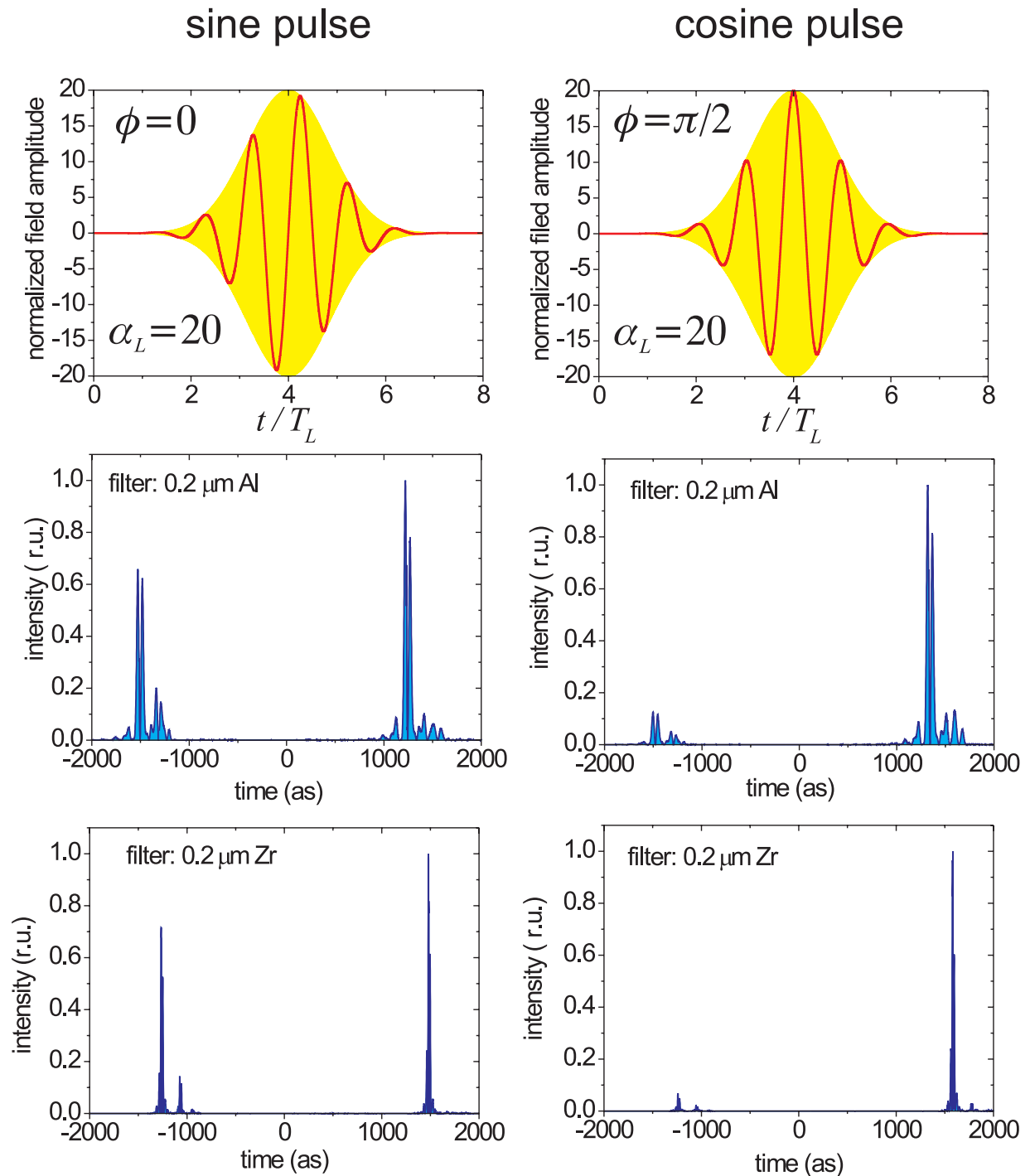


Figure 10. LPIC simulations for two different values of the envelope-carrier phase ϕ and for a Al and Zr filter. In the upper two diagrams, the normalized field amplitude with respect to the pulse envelope for the two types of pulses (sine and cosine) is shown. It is seen that the cosine pulse suppresses almost entirely one of the attosecond pulse produced thus generating a single attosecond pulse.

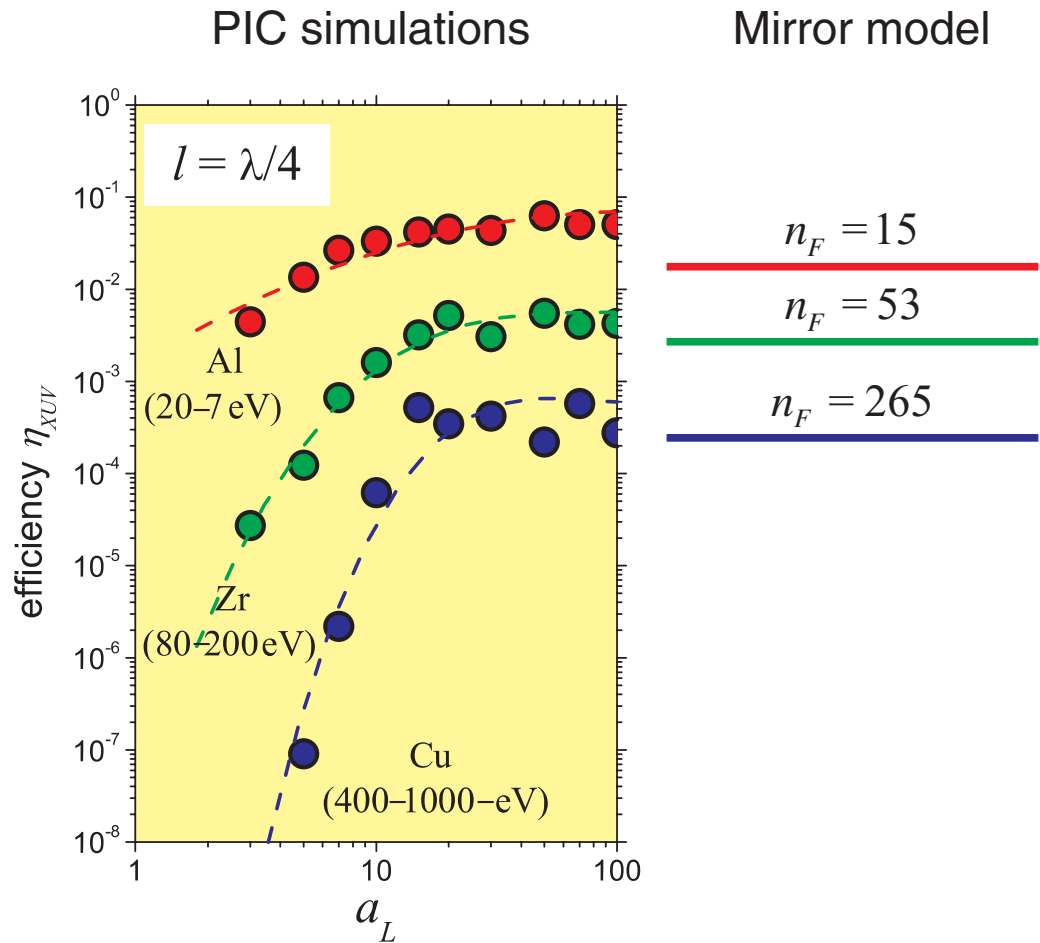


Figure 11. Variation of the XUV pulse efficiency η_{XUV} with the normalized vector potential a_L for three different spectral ranges determined by the indicated thin filter used. For comparison the saturation values for the efficiency predicted by the mirror model $\eta_{\text{XUV}} \rightarrow 1/n_F^{3/2}$ with n_F the low-energy cut-off of the corresponding filter is shown.

The extraordinary high efficiency of the generated attosecond XUV pulses is most striking. For 20–70 eV photon energy the conversion reaches the few per cent level while for the 400–1000 eV range and for $a_L \gtrsim 10$ the 10^{-4} level. As seen in figure 11, for large values of a_L the XUV pulse efficiency tends to level off but this occurs earlier for the low and progressively extends to high photon energy XUV pulses. It is noted that the saturation values predicted by the oscillating mirror model are borne out by simulations with the LPIC code. This is depicted also in figure 11 where the saturation values obtained from the simple expression $\eta_{\text{XUV}} \rightarrow 1/n_F^{3/2}$ for n_F the cut-off harmonic of the corresponding filter are indicated as straight horizontal lines. It is interesting to note that for the case of Zr filter, the corresponding conversion efficiency from gas harmonics at the maximum allowed intensity of $\simeq 10^{14} \text{ W cm}^{-2}$ is estimated to be only $\simeq 10^{-8}$ [33]. Given the facts that the incident pulse intensity is several orders of magnitude higher ($\simeq 10^{20}$ versus $10^{14} \text{ W cm}^{-2}$) and the efficiency is a factor of 10^4 larger than in the case of gas

harmonics, this opens up the possibility of generating single attosecond pulses at vastly higher intensities.

4. Discussion and conclusions

The results obtained in these feasibility study are certainly very encouraging with a great deal of scientific potential. The question that arises is to what extent this potential can be exploited and what are the main obstacles. For one thing, the theoretical treatment of the generation process of harmonics from overdense plasma reveals that there is no fundamental limitation in using the highest possible laser intensities available, i.e. no upper limit in the intensity is imposed by the nonlinear medium as in the case of atomic harmonics where ionization gives rise to the saturation intensity. On the contrary, the higher the laser intensity the stronger the nonlinear response of the medium.

The limitations appear to be more or less of technological nature related to the development of the high-power laser systems. Although high repetition laser systems capable of delivering intensities $\lesssim 10^{20} \text{ W cm}^{-2}$ are available today and the prospect of reaching the $10^{22} \text{ W cm}^{-2}$ intensity level is good, there will be more development necessary to effectively control the purity of the laser pulses generated regarding pedestal level and pre-pulses. Laser pulses with excessive background create a pre-plasma with a long scale-length so that the main laser pulse interacts with an expanded plasma. In the case of relatively low intensity $\lesssim 10^{18} \text{ W cm}^{-2}$ interactions, this has been shown to have a detrimental effect on the harmonic efficiency [15]. However, some preliminary simulation results for high intensity ($\geq 10^{19} \text{ W cm}^{-2}$) interaction with preformed plasmas indicate that the degradation of the efficiency for long scale-length plasmas is not as pronounced. If indeed this is the case, the next question is whether 2D effects like the ‘rippling’ of the critical surface would occur as in the case of older long pulse (ns–ps) experiments [34]–[36].

A factor that can counteract this possibility is the shortness of the laser pulse envisaged in this report. The ‘rippling’ of the critical surface is attributed mainly to the Rayleigh–Taylor instability. For laser pulses of 5 fs durations the classical Rayleigh–Taylor instability is not relevant since it presumes ion motion. In general, due to the shortness of the laser pulses considered here, it is expected that the critical surface would remain planar during the interaction period even for electron Rayleigh–Taylor-like instabilities reported by Wilks *et al* [37]. A related aspect is the deformation of the wave front of the incident pulse. If the pulses delivered by the high-intensity laser systems possess a deformed wave front this will affect the coherence of the individual sources contributing to the reflected pulse with the consequence of destroying the temporal localization and thus broadening the filtered pulses. These are 3D effects and can be studied only with simulations relying on at least 2D PIC codes.

A challenge that has to be dealt with is the characterization of the attosecond pulses. Fortunately, a number of techniques have been already developed for the characterization of similar pulses from gas harmonics. For the characterization of low photon energy attosecond pulses, the newly developed technique of volume autocorrelation [11] appears to be most appropriate. In this technique, the attosecond pulse is divided into two replicas by a split mirror arrangement that focuses the XUV beam into a He gas jet. The relative motion of the two parts of the mirror in small steps results in a rearrangement of the intensity distribution at the focus. If a two-photon ionization process takes place in the He gas [38], this change in distribution

gives rise to a modulation of the ion signal. Although some modification would be necessary to accommodate the broader spectrum from the few-cycle laser pulses, this technique could provide information on the temporal structure of the attosecond burst and how it changes when going from a sine to a cosine laser pulse. Additionally, and chiefly for synthesis of higher harmonics, the technique of the attosecond streak camera [39, 40] appears more appropriate. This is basically a cross-correlation technique, but it relies on a time reference given not by the envelope of the laser pulse, but instead by the oscillating field of the laser field itself to extract the duration of the XUV burst. It is suitable for XUV pulse durations shorter than a half-period of the oscillating laser field and it can be used to additionally measure the chirp of the attosecond pulse. Whenever possible, a comparison of the results obtained with the two techniques (volume autocorrelation and attosecond streak camera) would add reliability to the measurements.

A laser system delivering pulses of $E_L = 1$ J energy in $\tau_L = 5$ fs and focusable to a $10 \mu\text{m}$ spot produces intensities of $\sim 10^{20} \text{ W cm}^{-2}$. The simulations presented here indicate that generating harmonics in a plasma-vacuum interface with this laser system and using $0.2 \mu\text{m}$ Al foil to filter the reflected pulses, XUV pulses in the 20–70 eV photon energy range with 84 as duration containing 10^{16} photons are produced. The method proposed in this feasibility study compares favourably with the capabilities of the XUV x-ray free-electron laser (XUV-XFEL) currently in operation at the German Electron Synchrotron laboratory (DESY) in Hamburg [41]. The main difference being that since the pulses thus produced are much shorter, they are necessarily not as monochromatic as those obtained from the XFEL. However, the temporal resolution is accordingly superior and appropriate for investigations of very fast dynamical processes. Assuming that laser systems delivering high contrast pulses and focusable to very high intensities $\gtrsim 10^{22} \text{ W cm}^{-2}$ become available use of thicker and/or harder filters would result in pulses of unprecedented shortness taking us into the realm of zeptosecond durations.

Acknowledgments

We thank E Goulielmakis, S Gordienko and A Pukhov for fruitful discussions. This work is supported in part by the European Community's Human Potential Programme under contract MRTN-CT-2003-505138 (XTRA), the Commission of the EC within the framework of the Association Euratom-Max-Planck-Institut für Plasmaphysik and the Deutsche Forschungsgemeinschaft in the framework of SFB/TRANSREGIO contract.

References

- [1] Farkas Gy and Toth Cs 1992 *Phys. Lett. A* **168** 447
- [2] Harris S E, Macklin J J and Hänsch T W 1993 *Opt. Commun.* **100** 487
- [3] L'Huillier A and Balcou Ph 1993 *Phys. Rev. Lett.* **70** 774
- [4] Macklin J J, Kmetec J D and Gordon C L III 1993 *Phys. Rev. Lett.* **70** 766
- [5] Sarachik E S and Schappert G T 1970 *Phys. Rev. D* **1** 2738
- [6] Phuoc Ch K Ta, Rousse A, Pittman M, Rousseau J P, Malka V, Fritzler S, Umstadter D and Hulin D 2003 *Phys. Rev. Lett.* **91** 195001
- [7] Plaja L, Roso L, Rzazewski K and Lewenstein M 1998 *J. Opt. Soc. Am. B* **15** 1904

- [8] Hentschel M, Kienberger R, Spielmann Ch, Reider G A, Milosevic N, Brabec T, Corkum P, Heinzmann U, Drescher M and Krausz F 2001 *Nature* **414** 509
- [9] Kienberger R *et al* 2004 *Nature* **427** 817
- [10] Paul P M, Toma E S, Breger P, Mullot G, Auge F, Balcou Ph, Muller H G and Agostini P 2001 *Science* **292** 1690
- [11] Tzallas P, Charalambidis D, Papadogiannis N A, Witte K and Tsakiris G D 2003 *Nature* **426** 267
- [12] Drescher M, Hentschel M, Kienberger R, Uiberacker M, Yakovlev V, Scrinzi A, Westerwalbesloh Th, Kleineberg U, Heinzmann U and Krausz F 2002 *Nature* **419** 803
- [13] Kohlweyer S, Tsakiris G D, Wahlström C-G, Tillman C and Mercer I 1995 *Opt. Commun.* **111** 431
- [14] von der Linde D, Enders T, Jenke G, Agostini P, Grillon G, Nibbering E and Antonetti A 1995 *Phys. Rev. A* **52** R25
- [15] Zepf M *et al* 1998 *Phys. Rev. E* **58** R5253
- [16] Dubietis A, Jonusauskas G and Piskarskas A 1992 *Opt. Commun.* **88** 437
- [17] Zinkstok R Th, Witte S, Hogervorst W and Eikema K S E 2005 *Opt. Lett.* **30** 78
- [18] Ishii N *et al* 2005 *Opt. Lett.* **30** 567
- [19] Witte S, Zinkstok R Th, Hogervorst W and Eikema K S E 2005 *Opt. Express* **13** 4903
- [20] Tavella F, Schmid K, Ishii N, Marcinkevicius A, Veisz L and Krausz F 2005 *Appl. Phys. B* **81** 753
- [21] Baltuška A *et al* 2003 *Nature* **421** 611
- [22] Goulielmakis E *et al* 2004 *Science* **305** 1267
- [23] Lichters R, Meyer-ter-Vehn J and Pukhov A 1996 *Phys. Plasmas* **3** 3425
- [24] Bahk S-W, Rousseau P, Planchon T A, Chvykov V, Kalintchenko G, Maksimchuk A, Mourou G A and Yanovsky V 2005 *Appl. Phys. B* **80** 823
- [25] Naumova N M, Nees J A, Sokolov I V, Hou B and Mourou G A 2004 *Phys. Rev. Lett.* **92** 063902
- [26] Bulanov S V, Naumova N M and Pegoraro F 1994 *Phys. Plasmas* **1** 745
- [27] Gordienko S, Pukhov A, Shorokhov O and Baeva T 2004 *Phys. Rev. Lett.* **93** 115002
- [28] Meyer-ter-Vehn J, Pukhov A and Sheng Z M 2001 Relativistic laser plasma interaction *Atoms, Solids, and Plasmas in Super-Intense Laser Fields* vol 93, ed D Batani, C J Joachain, S Martellucci and A N Chester (New York: Kluwer) p 167
- [29] Watts I, Zepf M, Clark E L, Tatarakis M, Krushelnink K and Dangor A E 2002 *Phys. Rev. Lett.* **88** 155001
- [30] Teubner U *et al* 2003 *Phys. Rev. A* **68** 013816
- [31] Teubner U, Eidmann K, Wagner U, Andiel U, Pisani F, Tsakiris G D, Witte K, Meyer-ter-Vehn J, Schlegel T and Förster E 2004 *Phys. Rev. Lett.* **92** 185001
- [32] Christov I P, Murnane M M and Kapteyn H C 1997 *Phys. Rev. Lett.* **78** 1251
- [33] Schnürer M, Cheng Z, Hentschel M, Tempea G, Kálmán P, Brabec T and Krausz F 1999 *Phys. Rev. Lett.* **83** 722
- [34] Carman R L, Forslund D W and Kindel J M 1981 *Phys. Rev. Lett.* **46** 29
- [35] Norreys P A *et al* 1996 *Phys. Rev. Lett.* **76** 1832
- [36] Veres G, Bakos J S, Földes I B, Gál K, Juhász Z, Kocsis G and Szatmári S 1999 *Europhys. Lett.* **48** 390
- [37] Wilks S C, Krueer W L, Tabak M and Langdon A B 1992 *Phys. Rev. Lett.* **69** 1383
- [38] Papadogiannis N A, Nikolopoulos L A A, Charalambidis D, Tsakiris G D, Tzallas P and Witte K 2003 *Phys. Rev. Lett.* **90** 133902
- [39] Itatani J, Quéré F, Yudin G L, Ivanov M Yu, Krausz F and Corkum P B 2002 *Phys. Rev. Lett.* **88** 173903
- [40] Kitzler M, Milosevic N, Scrinzi A, Krausz F and Brabec T 2003 *Phys. Rev. Lett.* **88** 173904
- [41] Materlik G and Tschentscher Th (ed) 2001 *TESLA Technical Design Report, Part V, The X-ray Free Electron Laser* (Hamburg: DESY)